Modelling Solar Oscillation Power Spectra: III. Spatiotemporal spectra of solar granulation velocity field as seen in SDO HMI Doppler-velocity measurements

Sergei V. Vorontsov,[1,2] Stuart M. Jefferies,[3] and Timothy P. Larson[4]

[1]*Astronomy Unit, School of Physical and Chemical Sciences, Queen Mary University of London, Mile End Road, London E1 4NS, UK*
[2] *Institute of Physics of the Earth, B. Gruzinskaya 10, Moscow 123810, Russia*
[3]*Department of Physics and Astronomy, Georgia State University, Atlanta, GA, USA*
[4]*W.W. Hansen Experimental Physics Laboratory, Stanford University, Stanford, CA 94305-4085, USA*

ABSTRACT

We suggest a physically motivated model of the uncorrelated background, which can be used to improve the accuracy of helioseismic frequency measurements **when the background contributes significantly to the formation of spectral lines of acoustic resonances**. The basic assumption of our model is that the correlation length of the convective motions is small compared with horizontal wavelength $R_\odot/\ell$ of the observations, where ℓ is the degree of spherical harmonic $Y_{\ell m}(\theta, \varphi)$. When applied to solar power spectra at frequencies below acoustic resonances, the model reveals a distinct sensitivity to solar rotation: advection of the convective velocity pattern brings spatial correlations in the apparent stochastic velocity field (temporal correlations in the co-rotating frame induce spatial correlations in the inertial frame). The induced spatiotemporal correlations manifest themselves as an antisymmetric component in the dependence of the convective noise power on azimuthal order m, which allows us to address the solar differential rotation. With 360d power spectra measured with SDO HMI, three components of the rotation rate as a function of latitude can be evaluated in a single measurement at $\ell = 300$. This result indicates that the model suggests a new way of measuring solar subsurface rotation. This approach can complement traditional measurements based on correlation tracking.

Keywords: methods: data analysis — Sun: helioseismology — Sun: oscillations— Sun: rotation— Sun: convection

1. INTRODUCTION

The most challenging task in contemporary helioseismology is to reduce systematic errors in estimating solar p-mode frequencies. This problem stands up when analyzing long measurements, which can only reduce random errors. A large amount of data accumulated over the decades in dedicated ground-based and space projects calls for significantly improving the data analysis pipeline to exploit their full diagnostic potential. For a recent account of the available data and its processing, we refer the reader to Larson & Schou (2015, 2018) and Korzennik (2005, 2023).

Multiple sources of potential systematic errors come into play when we attempt to measure an oscillation frequency with accuracy better than the width of its resonant line in the observed power spectrum. Systematic offset is caused by inadequate modeling of the asymmetric line profile, inaccurate treatment of nearby spatial leaks (inaccuracies in the leakage matrix, which in turn has to account for possible instrumental and optical distortions and mode-coupling effects), incorrect magnitude and/or frequency gradient of the uncorrelated background noise.

This study is focused on global modeling of the uncorrelated background. It is common practice in the mode-fitting procedures to account for the uncorrelated background by simply allowing it as a single free parameter for each (n, ℓ) frequency multiplet to ensure numerical stability. When dependence on azimuthal order m is allowed, this dependence is evaluated by addressing a small frequency domain in the vicinity of resonances, a domain which is contaminated by unaccounted spatial leaks. We are looking for a possibility to describe the background in the entire range of (n, ℓ, m) globally by fitting a single slowly-varying function of frequency only.

It is natural to start with addressing noise power in the frequency range uncontaminated by global oscillation resonances (below 1mHz, where solar f- and p-modes are buried below the noise level). This study analyzes power spectra
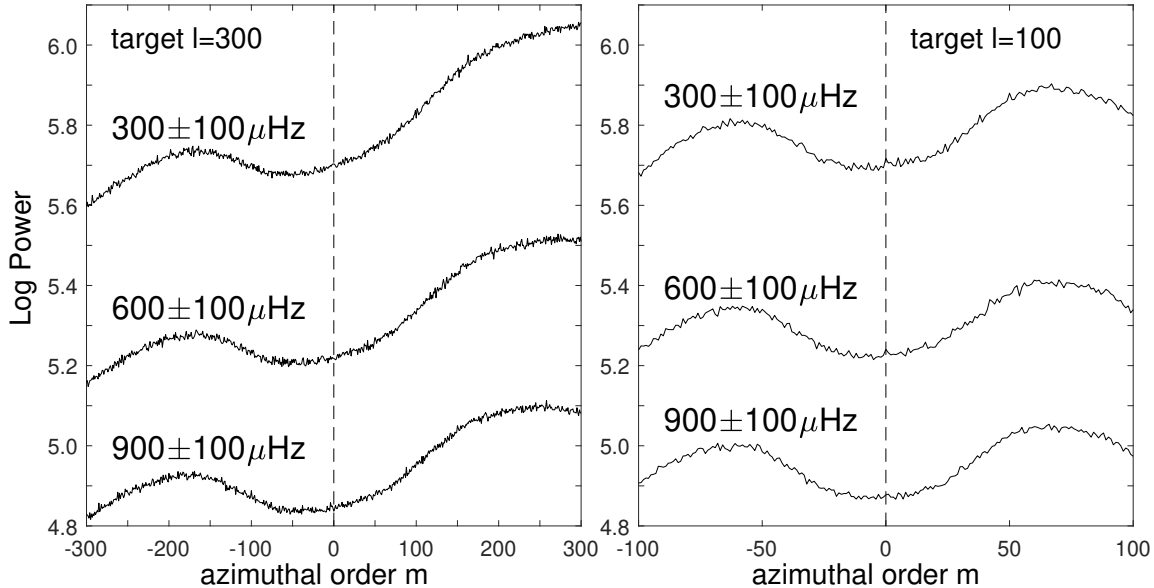
Figure 1. Observational noise power as function of azimuthal order m at $\ell = 300$ (left) and $\ell = 100$ (right) measured at frequencies around 300μHz, 600μHz and 900μHz.

obtained from **a 360 day-long time-series of Dopplergrams measured with Helioseismic and Magnetic Imager on board the Solar Dynamics Observatory** (taken from 2019.03.14 onwards, the one-year period centered on solar activity minimum). Figure 1 shows the observed power at degree $\ell = 300$ and $\ell = 100$ as a function of m at frequencies around 300μHz, 600μHz and 900μHz; the measurements were averaged over $\pm 100\mu$Hz frequency intervals.

We can make two interesting observations:

(i) For each of two values of degree ℓ, the three curves obtained at frequencies that differ by a factor three are essentially the same; the only difference is a nearly-uniform vertical shift on the logarithmic scale. This feature indicates that the functional dependence of the noise power on the spatial spectral numbers (ℓ, m) and temporal frequency ω is separable; and

(ii) the dependence on m is highly asymmetric. This feature points immediately to the effects of solar rotation, as the instrument's sensitivity does not depend on the sign of m. With our sign convention, harmonics with m positive are prograde waves, i.e., waves moving in the direction of rotation. In the co-rotating frame, these waves have a smaller frequency; the noise is higher at smaller frequencies.

Below is our attempt to understand this behavior in detail. In our vision, the noise comes from the turbulent convective velocity field in the solar photosphere. In Section 2, we analyze the spectral measures of this noise, assuming that the correlation length of the convective motions is small compared with observational wavelength $R_\odot/\ell$. We consider in detail the effects of differential rotation. Section 3 describes its measurement from the odd (in m) component of the noise power in SDO HMI measurements. We also analyze the even (in m) component, governed by different sensitivity of the instrument to different spatial harmonics of the velocity field. Extension of the leakage-matrix computations to include the instrument's response to torsional components of the velocity field, which enter the analysis, is described in Appendix. Section 4 suggests an initial approximation for the noise power in the frequency domain of acoustic resonances, which has to be iteratively improved when fitting solar power spectra in frequency measurements. Our results are discussed in Section 5.

2. SPECTRAL MEASURES OF GRANULATION VELOCITY FIELD IN SPATIAL AND TEMPORAL DOMAINS

We work in a spherical coordinate system (r, θ, φ) aligned with solar rotation axis, and expand the time-dependent surface velocity field $\mathbf{v}(\theta, \varphi, t)$ in vector spherical harmonics

$$\mathbf{v}(\theta, \varphi, t) = \sum_{\ell, m} [u_{\ell m}(t)\hat{r}Y_{\ell m}(\theta, \varphi) + v_{\ell m}(t)\nabla_1 Y_{\ell m}(\theta, \varphi) - w_{\ell m}(t)\hat{r} \times \nabla_1 Y_{\ell m}(\theta, \varphi)] \tag{1}$$

where ∇_1 is angular part of gradient operator, $\nabla_1 = \hat{\theta}\partial/\partial\theta + \sin^{-1}\theta\hat{\varphi}\partial/\partial\varphi$, hats designate unit vectors, and make a Fourier transform of the time string of some large length T

$$\int_0^T e^{i\omega t}\mathbf{v}(\theta,\varphi,t)dt = \sum_{\ell,m}\left[U_{\ell m}(\omega)\hat{r}Y_{\ell m}(\theta,\varphi) + V_{\ell m}(\omega)\nabla_1 Y_{\ell m}(\theta,\varphi) - W_{\ell m}(\omega)\hat{r}\times\nabla_1 Y_{\ell m}(\theta,\varphi)\right]. \tag{2}$$

Using orthogonality properties of vector spherical harmonics **and, throughout this paper, symbol ϖ to designate the solid angle (to avoid confusion with angular velocity),**

$$\int_{4\pi}\left[\nabla_1 Y_{\ell m}^*(\theta,\varphi)\right]\cdot\left[\nabla_1 Y_{\ell'm'}(\theta,\varphi)\right]d\varpi = \int_{4\pi}\left[-\hat{r}\times\nabla_1 Y_{\ell m}^*(\theta,\varphi)\right]\cdot\left[-\hat{r}\times\nabla_1 Y_{\ell'm'}(\theta,\varphi)\right]d\varpi = \ell(\ell+1)\delta_{\ell'\ell}\delta_{m'm}, \tag{3}$$

where star designates complex conjugate, we have

$$U_{\ell m}(\omega) = \int_0^T e^{i\omega t}u_{\ell m}(t)dt = \int_0^T e^{i\omega t}dt\int_{4\pi}\mathbf{v}(\theta,\varphi,t)\cdot\hat{r}Y_{\ell m}^*(\theta,\varphi)d\varpi, \tag{4}$$

$$\ell(\ell+1)V_{\ell m}(\omega) = \int_0^T e^{i\omega t}v_{\ell m}(t)dt = \int_0^T e^{i\omega t}dt\int_{4\pi}\mathbf{v}(\theta,\varphi,t)\cdot\nabla_1 Y_{\ell m}^*(\theta,\varphi)d\varpi, \tag{5}$$

$$\ell(\ell+1)W_{\ell m}(\omega) = \int_0^T e^{i\omega t}w_{\ell m}(t)dt = \int_0^T e^{i\omega t}dt\int_{4\pi}\mathbf{v}(\theta,\varphi,t)\cdot\left[-\hat{r}\times\nabla_1 Y_{\ell m}^*(\theta,\varphi)\right]d\varpi, \tag{6}$$

these expressions are obtained by taking scalar product of both sides of Equation (1) with $\hat{r}Y_{\ell'm'}^*(\theta,\varphi)$, $\nabla_1 Y_{\ell'm'}^*(\theta,\varphi)$, and $-\hat{r}\times\nabla_1 Y_{\ell'm'}^*(\theta,\varphi)$, integrating in angular coordinates and taking the Fourier transform.

We assume $\mathbf{v}(\theta,\varphi,t)$ to be a particular realization of a stationary stochastic process with zero mean. Quantities in the left-hand sides of Equations (4-6), represented by stochastic integrals in the right-hand sides, are thus random variables with zero mean, $\mathrm{E}[U_{\ell m}(\omega)] = \mathrm{E}[V_{\ell m}(\omega)] = \mathrm{E}[W_{\ell m}(\omega)] = 0$. We are interested in evaluating their variances $\mathrm{Var}U_{\ell m}(\omega) = \mathrm{E}[U_{\ell m}(\omega)^*U_{\ell m}(\omega)]$, $\mathrm{Var}V_{\ell m}(\omega)$ and $\mathrm{Var}W_{\ell m}(\omega)$, together with non-zero covariances, if any.

We associate $\mathbf{v}(\theta,\varphi,t)$ with the turbulent velocity field of convective motions imposed on a stationary large-scale background flow produced by differential rotation and meridional circulation. The basic assumption of our model is that for an observer moving together with the background flow, the convective velocities do not correlate in space. When addressing the granulation velocity field, this assumption can only be relevant in a limited range of spherical harmonic degree ℓ, when a typical size of a granule is small compared with horizontal wavelength $R_\odot/\ell$ (we will be working with Doppler-velocity power spectra in the degree range $0 \leq \ell \leq 300$). In this paper, we limit our analysis to the background flow produced by differential rotation only: the effects of meridional circulation require a different treatment and will be left for further studies.

To make derivations more transparent, we consider a model with the effects of rotation discarded before generalizing the results to include the effects of solid-body rotation and then differential rotation.

(i) *Non-rotating Sun.* Changing the order of integration, we rewrite Equation (4) as

$$U_{\ell m}(\omega) = \int_{4\pi}Y_{\ell m}^*(\theta,\varphi)\tilde{v}_r(\theta,\varphi,\omega)d\varpi, \tag{7}$$

where $\tilde{v}_r(\theta,\varphi,\omega)$ stands for the Fourier transform of radial velocity, $\tilde{v}_r(\theta,\varphi,\omega) = \int_0^T e^{i\omega t}v_r(\theta,\varphi,t)dt$, and consider the covariance

$$\mathrm{Cov}\left[\mathrm{U}_{\ell m}(\omega),\mathrm{U}_{\ell'm'}(\omega)\right] = \mathrm{E}\left[\int_{4\pi}\mathrm{Y}_{\ell m}(\theta,\varphi)\tilde{v}_r^*(\theta,\varphi,\omega)d\varpi \times \int_{4\pi}\mathrm{Y}_{\ell'm'}^*(\theta,\varphi)\tilde{v}_r(\theta,\varphi,\omega)d\varpi\right]. \tag{8}$$

Considering each of the two integrals on the right-hand side as a sum of integrals over small angular areas $\Delta\varpi_i$, and using indexing $\Delta\varpi_j$ to enumerate these areas in the same order in the second integral, we notice that the result is only contributed by diagonal elements $i = j$; expectation value of the cross-terms is zero because $\tilde{v}_r$-values do not correlate in space. We also know that the variance has an additive property. Therefore, if we replace the entire integration

4

domain 4π in the right-hand side of Equation (8) by a small angular element $\Delta\varpi$, the result will be proportional to $\Delta\varpi$. We thus have

$$\text{Cov}\left[U_{\ell m}(\omega), U_{\ell'm'}(\omega)\right] = \int_{4\pi} Y_{\ell m}(\theta, \varphi) Y^*_{\ell'm'}(\theta, \varphi) \sigma_r^2(\omega) d\varpi = \delta_{\ell'\ell}\delta_{m'm}\sigma_r^2(\omega), \tag{9}$$

where

$$\sigma_r^2(\omega) = \lim_{\Delta\varpi\to 0} \frac{1}{\Delta\varpi} \text{E}\left[\int_{\Delta\varpi} \tilde{v}_r^*(\theta, \varphi)\tilde{v}_r(\theta, \varphi) d\varpi\right] \tag{10}$$

is positive spectral measure of the variance of vertical velocities, which we assume to be uniform over the solar surface.

We work in a similar manner with contribution of horizontal components of the velocity field $v_\theta(\theta, \varphi, t)$ and $v_\varphi(\theta, \varphi, t)$ which have corresponding Fourier transforms $\tilde{v}_\theta(\theta, \varphi, \omega)$ and $\tilde{v}_\varphi(\theta, \varphi, \omega)$. We assume that horizontal velocities are isotropic in azimuthal direction and, therefore, the two orthogonal horizontal components do not correlate with each other and

$$\sigma_\theta^2(\omega) = \sigma_\varphi^2(\omega) = \frac{1}{2}\sigma_h^2(\omega), \tag{11}$$

where $\sigma_h^2(\omega)$ is spectral measure of absolute values of horizontal velocities. The result is

$$\text{Cov}\left[V_{\ell m}(\omega), V_{\ell'm'}(\omega)\right] = \text{Cov}\left[W_{\ell m}(\omega), W_{\ell'm'}(\omega)\right] = \frac{1}{2\ell(\ell+1)}\delta_{\ell'\ell}\delta_{m'm}\sigma_h^2(\omega) \tag{12}$$

(at $\ell = 0$, the horizontal components are identically zero).

We expect no correlation between U, V and W - contributions: the evidence comes from orthogonality of corresponding velocity components and symmetry considerations. Indeed, let $\mathbf{v}$ be velocity vector at a particular point on the solar surface, with $v_r = v \cdot \hat{r}Y_{\ell,m}(\theta, \varphi)$ and $v_h = v \cdot \nabla_1 Y_{\ell',m'}(\theta, \varphi)$. From geometrical considerations, the joint probability density function $p(v_r, v_h)$ is symmetric in v_h, i.e. for any value of v_r, two events with v_h of the same magnitude but of opposite sign have the same probability. The expectation value of their product $\text{E}(v_r v_h) = 0$, and hence there is no correlation between $U_{\ell,m}$ and $V_{\ell',m'}$. The same arguments apply to $U - W$ and $V - W$ pairs.

We now extend the analysis to include the effects of rotation.

(ii) *Solid-body rotation.* In this scenario, the Sun rotates with uniform angular velocity Ω in the observational frame. We assume that in the co-rotating frame, the **observable statistical properties of** convective motions are not influenced by the rotation **(influence of Coriolis forces on the velocity field on the horizontal scale of solar granulation is expected to be smeared away by spatial averaging)**. When the convective velocity field is observed in another reference frame, the only change is due to advection: in the spherical-harmonic decomposition, a component of azimuthal order m will have its temporal frequency shifted by $m\Omega$. The net result is that $\sigma_r^2(\omega)$ in Equation (9) has to be replaced with $\sigma_r^2(\omega - m\Omega)$, and similar with $\sigma_h^2(\omega)$ in Equation (12).

(iii) *Differential rotation.* We now allow the rotation to change with latitude. When the rotation is uniform, the variance of $U_{\ell m}(\omega)$ can be written as

$$\text{Var}\, U_{\ell m}(\omega) = \frac{2\ell+1}{2}\frac{(\ell-m)!}{(\ell+m)!}\int_{-1}^{1} [P_\ell^m(z)]^2\, \sigma_r^2(\omega - m\Omega)\, dz, \quad z = \cos\theta. \tag{13}$$

Since contributions to the variance coming from different latitudes simply add up, the same expression will be valid when Ω in the right-hand side is allowed to depend on latitude **(we can divide the spherical surface into thin latitudinal belts and assign individual co-rotating frame to each belt separately)**. We will assume now that the rotation is slow; limiting the analysis by terms linear in Ω,

$$\sigma_r^2\left(\omega - m\Omega(z)\right) = \sigma_r^2(\omega) - m\frac{d\sigma_r^2}{d\omega}\Omega(z), \tag{14}$$

and hence

$$\text{Var}\, U_{\ell m}(\omega) = \sigma_r^2\left(\omega - m\frac{2\ell+1}{2}\frac{(\ell-m)!}{(\ell+m)!}\int_{-1}^{1} [P_\ell^m(z)]^2\, \Omega(z)\, dz\right), \tag{15}$$

where $P_\ell^m(z)$ are associated Legendre polynomials.

Following an approach which is standard in solar seismology, we represent $\Omega(z)$ by an expansion

$$\Omega(z) = \sum_{s=1,3,5,\ldots} \Omega_s \frac{dP_s(z)}{dz}, \tag{16}$$

where $P_s(z)$ are Legendre polynomials (note that only even components of $\Omega(z)$ enter our result, as $[P_\ell^m(z)]^2$ is even function of z).

The required angular integrals are

$$m \frac{2\ell+1}{2} \frac{(\ell-m)!}{(\ell+m)!} \int_{-1}^{1} [P_\ell^m(z)]^2 \frac{dP_s(z)}{dz}\, dz = (-1)^{k+1} \frac{(\ell-1)!}{(\ell-k)!} \frac{(2\ell+1)!!}{(2\ell+2k-1)!!} \frac{(2k-1)!!}{(k-1)!} \mathcal{P}_{2k-1}^{(\ell)}(m)$$

$$= \left(\frac{4\pi}{2s+1}\right)^{1/2} \gamma_{s\ell}^m, \tag{17}$$

where $s = 2k-1$, $\gamma_{s\ell}^m$ are odd polynomials of degree s in m defined in (Ritzwoller & Lavely 1991) and $\mathcal{P}_{2k-1}^{(\ell)}(m)$ are polynomials currently used in solar seismology to describe frequency splittings of solar oscillations, following normalization defined in (Schou et al. 1994). Equation (17) can be derived by expanding $dP_s(z)/dz$ in $P_i(z)$, $i < s$, and evaluating integrals of triple products of Legendre polynomials. Convenient recurrence relations for evaluating $\mathcal{P}_{2k-1}^{(\ell)}(m)$ can be found in (Vorontsov 2007). We thus have

$$\operatorname{Var} U_{\ell m}(\omega) = \sigma_r^2 \left[\omega - \sum_{s=1,3,\ldots} \left(\frac{4\pi}{2s+1}\right)^{1/2} \gamma_{sl}^m \Omega_s\right]. \tag{18}$$

Introducing a-coefficients, commonly used in solar seismology, we have

$$\mathbf{Var}\, U_{\ell m}(\omega) = \sigma_r^2 \left(\omega - \sum_{s=1,3,\ldots} 2\pi a_s \mathcal{P}_s^{(\ell)}(m)\right). \tag{19}$$

The relation between the expansion coefficients Ω_s and a_s is provided by Equation (17); in particular,

$$2\pi a_1 = \Omega_1, \quad 2\pi a_3 = -\frac{3(\ell-1)}{(2\ell+3)}\Omega_3, \quad 2\pi a_5 = \frac{15(\ell-1)(\ell-2)}{2(2\ell+3)(2\ell+5)}\Omega_5. \tag{20}$$

Variances of $V_{\ell m}(\omega)$ and $W_{\ell m}(\omega)$ (Equations 5, 6) are transformed by the effects of differential rotation in precisely the same way.

We have an interesting observation: under the effects of differential rotation, each spectral component of velocity variances "split" in its observed frequency in precisely the same way as an undistorted frequency of solar oscillations would split under the effects of the same differential rotation if the influence of Coriolis forces can be discarded (leaving effects of advection only) and differential rotation does not change with depth.

We also note that possible inaccuracy, introduced by linearization in the rotation rate (Equations 14, 15) can only affect the response to differential components. The response to the dominant Ω_1-component is treated correctly whatever its magnitude, because $(4\pi/(2s+1))^{1/2}\gamma_{s\ell}^m = m$ for $s = 1$.

3. SOLAR CONVECTIVE VELOCITY FIELD AS SEEN IN SDO HMI POWER SPECTRA

Instrumental response to different velocity field components does not depend on sign of azimuthal order m. Parameters of differential rotation (Equations 19, 20) can thus be addressed by shifting in frequency the power spectra of individual m-channels to eliminate the odd (in m) component of the noise power. This procedure was implemented iteratively to account for a finite frequency window ($\pm 100\mu$Hz in our measurement). The result obtained at $\ell = 300$ at frequencies around 900μHz is $a_1 = \Omega_1/(2\pi) = 390.0 \pm 0.9$ nHz (synodic), $a_3 = 20.0 \pm 1.3$ nHz ($\Omega_3/(2\pi) = -13.4 \pm 0.9$ nHz), and $a_5 = 2.4 \pm 1.7$ nHz ($\Omega_5/(2\pi) = 1.3 \pm 0.9$ nHz). **To evaluate the quality of this fit, we use merit function defined as r.m.s. value of the residuals weighted with observational uncertainties, the uncertainties being evaluated under a standard assumption that observational power in an individual channel**

at individual frequency has χ^2-distribution with two degrees of freedom. Ideally, the value of this merit function shall be close to one. In our measurement, it is 1.073, which indicates that the targeted odd (in m) component is successfully eliminated in the "de-rotated" power spectra.

This result shall be compared with other available measurements. Helioseismic measurements of solar internal rotation lose their accuracy in the sub-surface layers, where the rotation varies rapidly with depth, and global modes lose their resolving power. However, the measurements reduced to solar activity minimum (Figure 8 of Vorontsov et al. 2002) indicate the surface values of $\Omega_1/(2\pi) \simeq 435$ nHz (sidereal, or synodic plus 31.6 nHz), $\Omega_3/(2\pi) \simeq -13$ nHz and $\Omega_5/(2\pi) \simeq 1$ nHz. The mean rotation rate Ω_1 inferred from the convective noise is thus about 13 nHz slower; Ω_3 and Ω_5 appear to be in perfect agreement.

A classical result of measuring solar differential rotation using correlation tracking (Snodgrass & Ulrich 1990) is

$$\Omega/(2\pi) = 0.473 - 0.077\cos^2\theta - 0.0575\cos^4\theta \ (\mu\text{Hz}) \tag{21}$$

sidereal, which translates to $\Omega_1/(2\pi) = 468.0$ nHz siderial, $\Omega_3/(2\pi) = -5.15$ nHz and $\Omega_5/(2\pi) = -1.46$ nHz. The variance with our measurement is much bigger here. One realistic scenario is that the measurements refer to different effective depths below the visible solar surface. The result of Snodgrass & Ulrich (1990), however, is hard to reconcile with results of helioseismic measurements (e.g., Vorontsov et al. 2002), where $\Omega_3/(2\pi) \simeq -14 \pm 1$nHz is found to be nearly constant with depth over the entire convective envelope, and $\Omega_1/(2\pi)$ increases with depth, reaching its maximum value (at a depth of about 6 percent of solar radius) of about 449 nHz (sidereal) only.

Accurate measurement of rotation of solar granulation pattern is quite demanding to data quality. It benefits from going to higher degree ℓ (allowing bigger and wider grid of azimuthal orders m), from observations with better spatial resolution (spatial leaks are not accounted for in the rotation measurement), and from observations of longer duration (better signal-to-noise ratio). When using 360d SDO HMI data, measurement of relatively small differential components of the rotation rate looses stability at degree ℓ less than about 200, leaving the possibility of evaluating mean rotation only. Power spectra of SOHO MDI "structure" program are not suitable for measurements at degree ℓ higher than 200 due to contamination by spatial leaks resulted from insufficient spatial resolution. For the same reason of limited spatial resolution, productive measurements of differential rotation would hardly be possible with currently available GONG data.

We have attempted a measurement identical to that described above at $\ell = 300$ but with SDO HMI 360d power spectra replaced by those of 63d run of SOHO MDI "dynamics" program (start date 1996.05.23). The result is $a_1 = 374.3 \pm 2.2$ nHz, $a_3 = 20.1 \pm 3.1$ nHz (a_5 is unstable due to the shorter observation). While the a_3 coefficient is in agreement with HMI measurement, the a_1 coefficient appears to be about 16 nHz smaller. In our vision, the difference comes from contamination of the MDI power spectra with bigger spatial leaks due to a smaller spatial resolution of the instrument. This explanation is confirmed by analyzing SDO HMI measurements performed with artificially degraded spatial resolution (Larson & Schou 2018). The difference can also be contributed by different depth of formation of spectral lines used by the two instruments: SOHO MDI was observing the Sun slightly higher in the atmosphere (Fleck et al. 2011).

With the odd (in m) component successfully eliminated in the properly "de-rotated" observational power spectra, we now analyze the remaining even component. For the same measurement at $\ell = 300$ and frequencies $900 \pm 100\mu$Hz, this component is shown by a thin line in Figure 2, where **the remaining even component of the observed power**

$$B_{\ell m}^2(\omega) = B_l^2(m)\overline{B}^2(\omega) \tag{22}$$

is represented **by the dimensionless variable $B_l^2(m)$ in units of $\overline{B}^2(\omega)$, which is m-averaged value of $B_{\ell m}^2(\omega)$.**

Contribution of the convective velocity field to the observational power spectra comes through multiple $U_{\ell m}$, $V_{\ell m}$ and $W_{\ell m}$-components (Equations 4-6). As signals coming through these components do not correlate with each other, we have, for the "de-rotated" power spectra,

$$B_{\ell m}^2(\omega) = \sigma_r^2(\omega)\sum_{\ell' m'}\left|R_{\ell'\ell}^{m'm}\right|^2 + \frac{\sigma_h^2(\omega)}{2\ell(\ell+1)}\left[\sum_{\ell' m'}\left|H_{\ell'\ell}^{m'm}\right|^2 + \sum_{\ell' m'}\left|T_{\ell'\ell}^{m'm}\right|^2\right], \tag{23}$$

where we introduce the notation R, H, and T to designate separate leakage matrices which specify sensitivity coefficients of the instrument to radial components of the velocity field, horizontal components of the poloidal vector fields, and
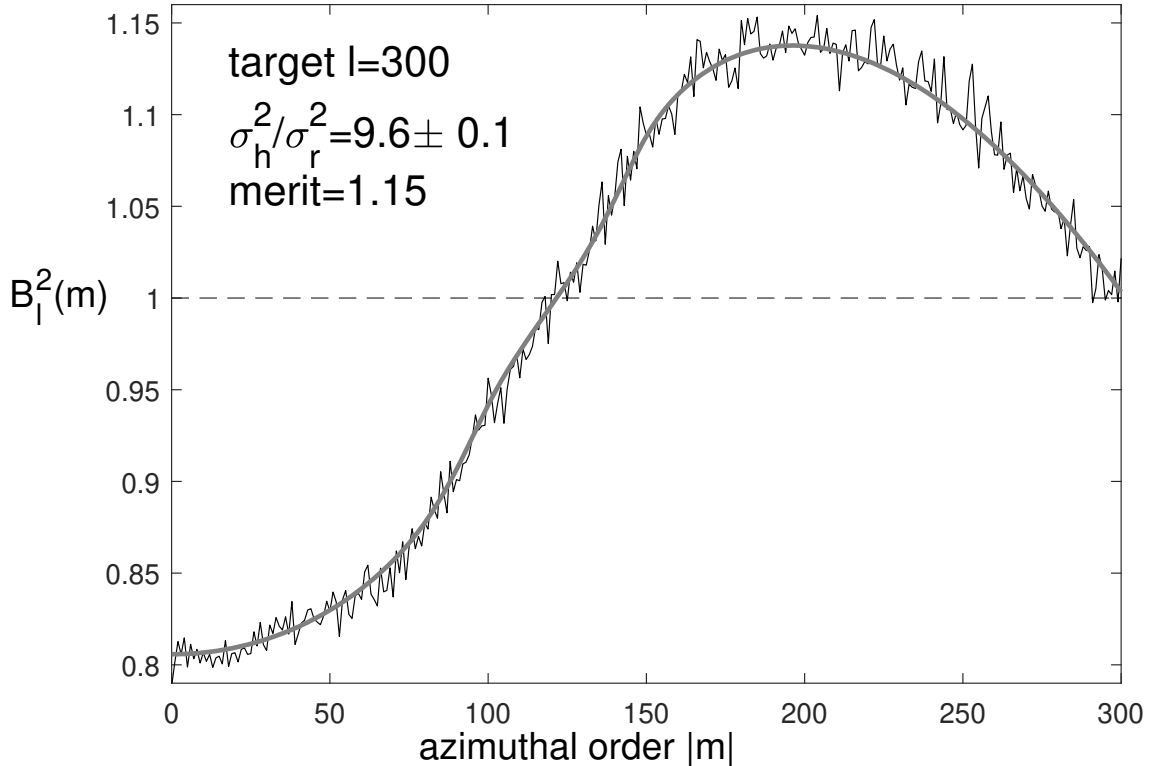
Figure 2. Even component in the observational noise power as function of azimuthal order m at $l = 300$ measured at frequencies around 900μHz (thin line). Thick gray line shows its approximation obtained by fitting synthetic power.

components of the toroidal fields (Equation 1), respectively. To make sure that sufficient amount of spectral leaks are accounted for, the leakage matrices were computed with ℓ' in the range $\ell \pm 30$ and $m' = m \pm 30$. Computation of the leakage matrices followed a semi-analytic approach described in (Vorontsov & Jefferies 2005), which was generalized to include the instrument's response to toroidal velocity fields; the details can be found in Appendix. To account for a finite resolution of the instrument in the CCD plane, the leakage-matrix analysis involves convolution of the images with a 2D Gaussian point-spread function (PSF); when working with high-resolution HMI data in the intermediate-degree range $\ell \leq 300$, the width of the PSF was set to zero (infinite resolution, PSF described by 2D Dirac δ-function). Solar B-angle was set to 5.11 deg, the r.m.s. value of its annual variation (for a small B-angle, its effect is quadratic in its magnitude).

The observed power $B^2_{\ell m}(\omega)$ considered as a function of m at $\ell = 300$ is fitted by a linear combination of the two terms in the right-hand side of Equation (23) with unknown coefficients σ_r^2 and σ_h^2. The result is shown in Figure 2 by a thick gray line. Visual inspection of the fit quality and the value of the corresponding merit function indicate that the approximation of the measured function of m by a linear combination of two functions coming exclusively from leakage-matrix analysis is perfectly adequate. The inferred ratio $\sigma_h^2/\sigma_r^2 = 9.6 \pm 0.1$ indicates that horizontal velocities in the turbulent flow are about 3 times bigger than vertical velocities. The fit quality remains adequate when the same analysis is applied to data at a smaller degree ℓ. An interesting observation is that the measured ratio σ_h^2/σ_r^2 increases monotonically to 18.2 ± 0.5 at $\ell = 100$ and 20.5 ± 2.9 at $\ell = 5$ (at degree $\ell < 5$, this measurement loses stability due to an insufficient number of the available m-states). This finding may indicate that bigger convective cells have a bigger average ratio of horizontal to vertical velocities.

Another finding is that the observed m-averaged value $\overline{B}^2(\omega)$ stays nearly constant in the entire degree range: it drops monotonically when going from $\ell = 0$ to $\ell = 300$, but only by about 15 percent (for comparison, in medium-ℓ SOHO MDI measurements of much smaller spatial resolution, this variation amounts to two orders of magnitude). This behavior indicates that in the degree range of up to $\ell = 300$, the spatial resolution of the HMI instrument is indeed almost perfect. To clarify this point, our analysis can be made independent of the leakage-matrix computations—assuming, of course, that the spatial resolution of the instrument is perfect.

In addition to the coordinate system (θ, φ) with z-axis aligned with the solar rotation axis, we introduce another coordinate system (θ', φ') with z'-axis (from which θ' is counted) directed from the Sun towards the observer. Considering the projection of the turbulent velocity field $\mathbf{v}(\theta, \varphi, t)$ (Equation 1) on the CCD plane directly, without its decomposition in vector spherical harmonics, we have

$$B_{\ell m}^2(\omega) = \mathrm{E} \left| \int_{4\pi} Y_{\ell m}^*(\theta, \varphi) \Pi(\sin \theta') \hat{z}' \cdot \tilde{\mathbf{v}}(\theta, \varphi, \omega) \, d\varpi \right|^2, \tag{24}$$

where $\tilde{\mathbf{v}}(\theta, \varphi, \omega)$ is Fourier transform of $\mathbf{v}(\theta, \varphi, t)$ at frequency shifted by advection effects, and $\Pi(\sin \theta')$ is apodization function, $\sin \theta'$ being radial coordinate in the image plane in units of the apparent solar radius. Evaluating the measure of the stochastic signal in the way described in Section 2 gives immediately

$$B_{\ell m}^2(\omega) = \int_{4\pi} Y_{\ell m}^*(\theta, \varphi) Y_{\ell m}(\theta, \varphi) \Pi^2(\sin \theta') \left[\cos^2 \theta' \sigma_r^2(\omega) + \frac{1}{2} \sin^2 \theta' \sigma_h^2(\omega) \right] d\varpi, \tag{25}$$

where $\cos^2 \theta'$ and $\sin^2 \theta'/2$ account for the line-of-sight projection effects. Using addition theorem for spherical harmonics, the m-averaged value is

$$\overline{B}^2(\omega) = \frac{1}{2\ell + 1} \sum_{m=-\ell}^{\ell} B_{\ell m}^2(\omega) = \frac{1}{4\pi} \int_{4\pi} \Pi^2(\sin \theta') \left[\cos^2 \theta' \sigma_r^2(\omega) + \frac{1}{2} \sin^2 \theta' \sigma_h^2(\omega) \right] d\varpi, \tag{26}$$

the result which does not depend on the target degree ℓ.

By expanding $\cos^2 \theta' \Pi^2(\sin \theta')$ and $\sin^2 \theta' \Pi^2(\sin \theta')$ in Equation (25) in spherical harmonics and transforming the result to (θ, φ)-coordinates, it is also possible to evaluate the right-hand side at individual m-values. We skip the details of this analysis, as its principal motivation was to check the accuracy of our leakage-matrix computations. The numerical results of the two approaches turned out to be the same.

The slight variation of the apparent values of $\overline{B}^2(\omega)$ with degree ℓ indicates that the leakage matrices can be improved by setting the PSF width to a small but non-zero value. We conclude that the measurements of the solar noise can be used to calibrate the effective PSF of the instrument. This option may be particularly interesting for analyzing data obtained with SOHO MDI instrument.

4. TEMPORAL DOMAIN

The m-average of the de-rotated (frequency-shifted according to the result of differential-rotation measurement) power spectra in the entire frequency domain of SDO HMI data at $\ell = 300$ is shown in Figure 3.

At frequencies less than about 200μHz, variation of the observed power with ℓ and m can not be explained by our model, which loses its ability to fit the data with any reasonable accuracy. In this spatiotemporal domain, our assumption of negligibly small correlation length is violated by supergranular-scale convective motions: Doppler-velocity power as function of m and ω is shown on a gray scale in Figure 4. The well-defined ridge at $m > 0$ (prograde waves) is produced by the rotation of solar supergranulation pattern. A small but noticeable curvature of the ridge is due to faster rotation of the equatorial regions. At frequencies less the about 50μHz, the observed power drops rapidly because of the de-trending implemented to the time-series of solar Dopplergrams.

In this study, the data analysis was limited by frequencies below the oscillation resonances. We can hope that the dependence of the noise power on ℓ and m (the $B_\ell^2(m)$) measured in this frequency range will stay the same at higher frequencies; this assumption, of course, remains to be verified by addressing residuals of spectral fitting procedures. We note that at frequencies from about 3 mHz and higher, the measurement of the background component is difficult because the signal-to-noise ratio of acoustic resonances becomes very high. At these frequencies, it is now the uncorrelated background which gets buried below the resonant power.

We suggest a simple model for the frequency dependence of the background noise $\overline{B}^2(\omega)$ to be used as an initial guess in the mode-fitting procedures. Imagine a convective eddy emerging on the solar surface from below at time $t = 0$. Let the observed velocity increases linearly with time and then drop exponentially,

$$v = \begin{cases} 0, & t < 0 \\ \frac{t}{\tau^2} e^{-\frac{t}{\tau}}, & t \geq 0. \end{cases} \tag{27}$$
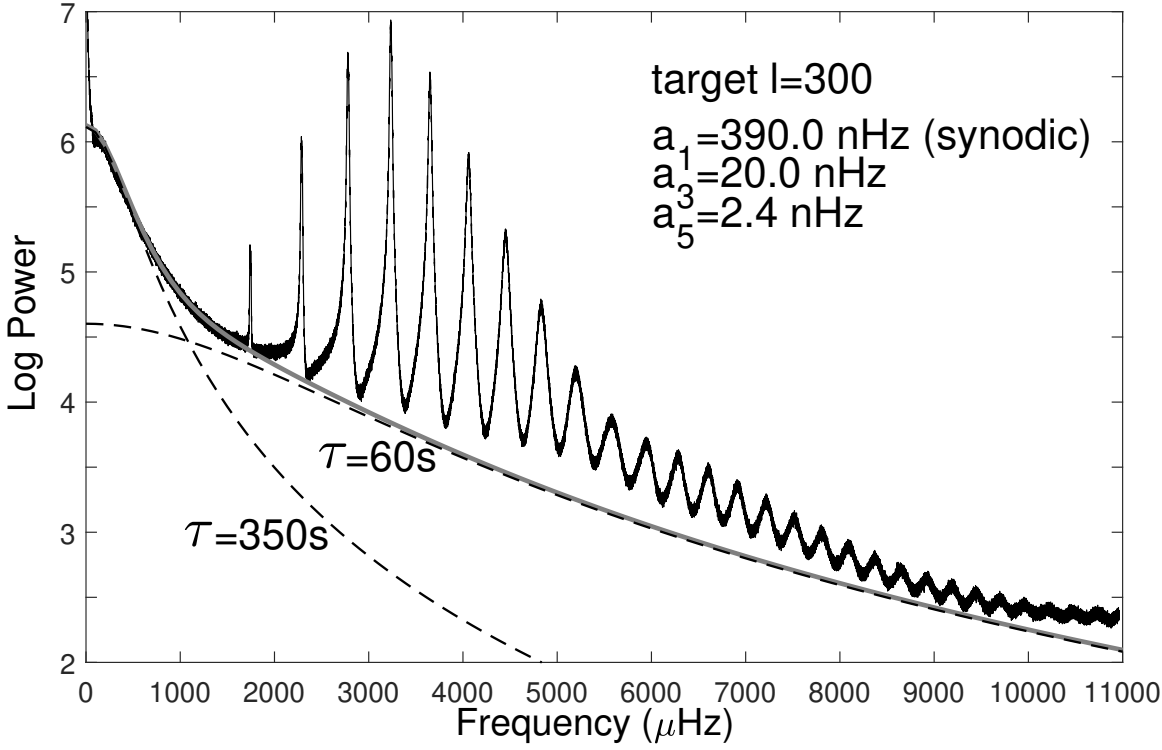
Figure 3. De-rotated and m-averaged SDO HMI power spectrum at $l = 300$ (thin line). Dashed lines show two simple models (see text); their sum is shown by the thick gray line.
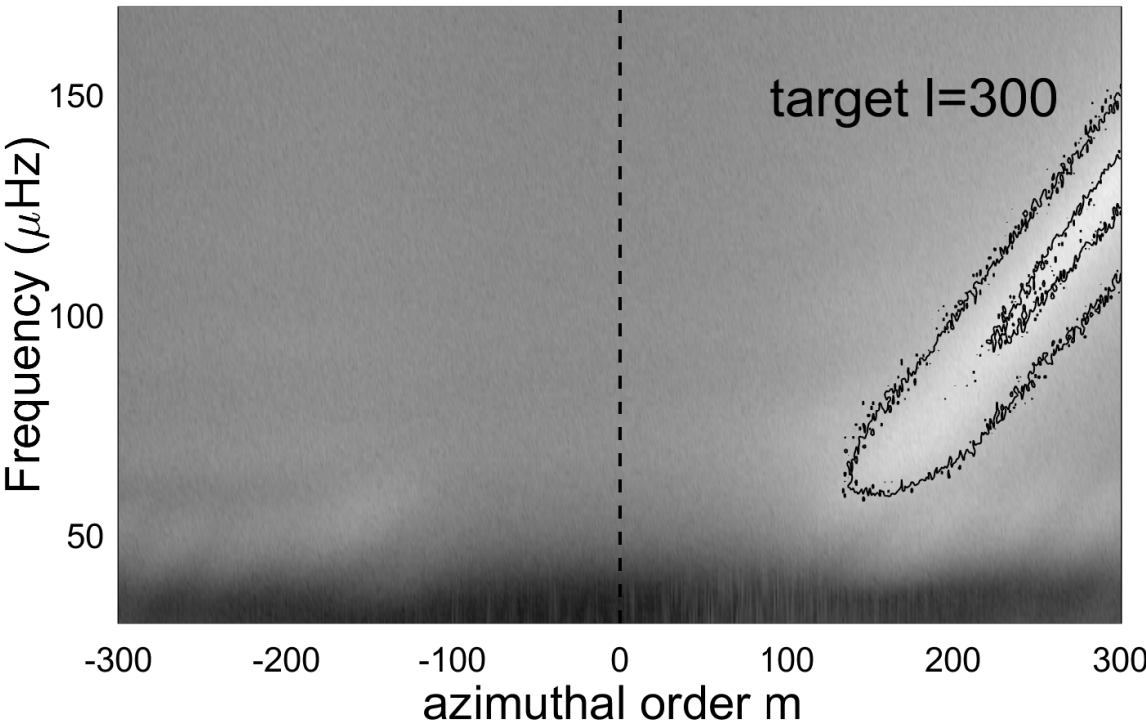
Figure 4. Velocity power at $\ell = 300$ and frequencies below 170 μHz.

Taking the Fourier transform, the observed power is $(1 + \omega^2\tau^2)^{-2}$. The Fourier power is a cosine Fourier transform of the autocorrelation function, which is

$$ACF = \frac{1}{4\tau}\left(1 + \left|\frac{t}{\tau}\right|\right)e^{-\left|\frac{t}{\tau}\right|}. \tag{28}$$

We adjust a linear combination of these "seismic events" with two different values of τ to approximate the expected variation of the uncorrelated background in the entire frequency range; the result is shown in Figure 3 by two dashed lines for the two separate components and by thick gray line for their sum. The fitted values of τ, about 6 mins and 1 min, are of the order of the lifetimes of solar granules and shorter. A relative excess of observational power at the highest frequencies may be due to an aliasing signal coming from frequencies higher than Nyquist frequency.

5. DISCUSSION

Implementation of our model in frequency measurements is relatively straightforward. At each degree, ℓ, the even functions $B_\ell^2(m)$ are measured from the de-rotated power spectra around some frequency below all the detectable resonances. The initial approximation for the frequency dependence of the uncorrelated background $\overline{B}^2(\omega)$ is then improved by fitting individual multiplets in the power spectra. When the instrument's resolution is imperfect (HMI measurements at higher degree ℓ or SOHO MDI measurements), the more minor sensitivity to modes of higher degree ℓ will be captured in $B_\ell^2(m)$.

The suggested measurement of differential rotation from power spectra at frequencies below the acoustic resonances will benefit from employing more data of smaller and higher degree ℓ analyzed in different frequency intervals. It is interesting to extend these measurements to datasets obtained at different times to explore temporal variations of the subsurface differential rotation ("torsional oscillations").

In our limited exercise with observational data, we have another finding which deserves more extensive data analysis. The inferred ratio of magnitudes of horizontal and vertical components of convective velocities σ_h^2/σ_r^2 clearly tends to get bigger when ℓ gets smaller; it indicates that in bigger convective cells, horizontal velocities become more dominant.

Our model becomes inconsistent with observations at frequencies from about 200μHz and below, since our basic assumption of small correlation length breaks down when observations start to feel signals from supergranular convective cells. Here, we enter the spatiotemporal domain targeted by Beck & Schou (2000) in their encouraging measurements of differential rotation of solar supergranulation pattern from Dopplergrams provided by SOHO MDI instrument. An approach which is more sophisticated than ours is needed to deal with turbulent-velocity correlations simultaneously in both space and time.

APPENDIX

The leakage matrices used in this study were calculated using the semi-analytic approach described in (Vorontsov & Jefferies 2005). This approach was extended in (Vorontsov & Jefferies 2013) to account explicitly for non-zero solar B-angle **(which is heliographic latitude of the central point of the solar disk)**. In this study, we need to develop the analysis further to include the instrument's response to components of the velocity field described by toroidal vector spherical harmonics. We have also noticed an inaccuracy in the earlier treatment of the B-angle effect (line-of-sight projection was done in the direction orthogonal to the solar rotation axis, thus missing the observer). Therefore, we outline the overall algorithm briefly, adding proper extensions.

We implement three separate leakage matrices—$R_{\ell'\ell}^{m'm}$, $H_{\ell'\ell}^{m'm}$ and $T_{\ell'\ell}^{m'm}$, with response coefficients to the vertical component of poloidal vector fields, to their horizontal component, and to the toroidal vector fields, respectively. We discard here all possible instrumental and optical distortions.

We choose the coordinate system (r, θ, φ) such that its z-axis is aligned with solar rotation, axis y is orthogonal to the line of sight, and axis x (from which φ is counted) is directed towards the observer when solar B-angle is zero. We choose another axis z', which points toward the observer. Angle β counted from z to z' is 90 degrees minus solar

B-angle. We start with a line-of-sight projection of the vector velocity fields: it will allow further analysis to work with scalar fields. The projection of vector $\mathbf{v}$ to the line of sight is

$$\hat{z}' \cdot \mathbf{v} = \sin\beta\,\hat{x}\cdot\mathbf{v} + \cos\beta\,\hat{z}\cdot\mathbf{v}. \tag{1}$$

For poloidal vector fields, we need an expansion in spherical harmonics of $\hat{x}\cdot\hat{r}Y_{\ell m}(\theta,\varphi)$, $\hat{z}\cdot\hat{r}Y_{\ell m}(\theta,\varphi)$, $\hat{x}\cdot\nabla_1 Y_{\ell m}(\theta,\varphi)$, and $\hat{z}\cdot\nabla_1 Y_{\ell m}(\theta,\varphi)$. These decompositions are (Vorontsov & Jefferies 2005):

$$\hat{x}\cdot\hat{r}Y_{\ell m}(\theta,\varphi) = -\frac{1}{2}\left[\frac{(\ell+m-1)(\ell+m)}{(2\ell-1)(2\ell+1)}\right]^{\frac{1}{2}} Y_{\ell-1,m-1}(\theta,\varphi) + \frac{1}{2}\left[\frac{(\ell-m-1)(\ell-m)}{(2\ell-1)(2\ell+1)}\right]^{\frac{1}{2}} Y_{\ell-1,m+1}(\theta,\varphi)$$
$$+ \frac{1}{2}\left[\frac{(\ell-m+1)(\ell-m+2)}{(2\ell+1)(2\ell+3)}\right]^{\frac{1}{2}} Y_{\ell+1,m-1}(\theta,\varphi) - \frac{1}{2}\left[\frac{(\ell+m+1)(\ell+m+2)}{(2\ell+1)(2\ell+3)}\right]^{\frac{1}{2}} Y_{\ell+1,m+1}(\theta,\varphi), \tag{2}$$

$$\hat{z}\cdot\hat{r}Y_{\ell m}(\theta,\varphi) = \left[\frac{(\ell+m)(\ell-m)}{(2\ell-1)(2\ell+1)}\right]^{\frac{1}{2}} Y_{\ell-1,m}(\theta,\varphi) + \left[\frac{(\ell+m+1)(\ell-m+1)}{(2\ell+1)(2\ell+3)}\right]^{\frac{1}{2}} Y_{\ell+1,m}(\theta,\varphi), \tag{3}$$

$$\hat{x}\cdot\nabla_1 Y_{\ell m}(\theta,\varphi) = -\frac{\ell+1}{2}\left[\frac{(\ell+m-1)(\ell+m)}{(2\ell-1)(2\ell+1)}\right]^{\frac{1}{2}} Y_{\ell-1,m-1}(\theta,\varphi) + \frac{\ell+1}{2}\left[\frac{(\ell-m-1)(\ell-m)}{(2\ell-1)(2\ell+1)}\right]^{\frac{1}{2}} Y_{\ell-1,m+1}(\theta,\varphi)$$
$$-\frac{\ell}{2}\left[\frac{(\ell-m+1)(\ell-m+2)}{(2\ell+1)(2\ell+3)}\right]^{\frac{1}{2}} Y_{\ell+1,m-1}(\theta,\varphi) + \frac{\ell}{2}\left[\frac{(\ell+m+1)(\ell+m+2)}{(2\ell+1)(2\ell+3)}\right]^{\frac{1}{2}} Y_{\ell+1,m+1}(\theta,\varphi), \tag{4}$$

$$\hat{z}\cdot\nabla_1 Y_{\ell m}(\theta,\varphi) = (\ell+1)\left[\frac{(\ell+m)(\ell-m)}{(2\ell-1)(2\ell+1)}\right]^{\frac{1}{2}} Y_{\ell-1,m}(\theta,\varphi) - \ell\left[\frac{(\ell+m+1)(\ell-m+1)}{(2\ell+1)(2\ell+3)}\right]^{\frac{1}{2}} Y_{\ell+1,m}(\theta,\varphi). \tag{5}$$

Corresponding expressions for toroidal vector spherical harmonics are derived in the same way; the result is

$$\hat{x}\cdot[-\hat{r}\times\nabla_1 Y_{\ell m}(\theta,\varphi)] = -\frac{i}{2}\left[(\ell+m)(\ell-m+1)\right]^{\frac{1}{2}} Y_{\ell,m-1}(\theta,\varphi) - \frac{i}{2}\left[(\ell-m)(\ell+m+1)\right]^{\frac{1}{2}} Y_{\ell,m+1}(\theta,\varphi), \tag{6}$$

$$\hat{z}\cdot[-\hat{r}\times\nabla_1 Y_{\ell m}(\theta,\varphi)] = -im Y_{\ell,m}(\theta,\varphi). \tag{7}$$

The rest of the analysis is the same as in (Vorontsov & Jefferies 2005, 2013): we rotate the coordinate system by angle β to direct axis z towards the observer, convolve the image with PSF in the apodization domain, and rotate the coordinate system back to its original orientation. Symmetry relations for the resulted leakage matrices are

$$R_{\ell'\ell}^{-m',-m}(\beta) = (-1)^{m'+m} R_{\ell'\ell}^{m'm}(\beta), \quad H_{\ell'\ell}^{-m',-m}(\beta) = (-1)^{m'+m} H_{\ell'\ell}^{m'm}(\beta),$$
$$T_{\ell'\ell}^{-m',-m}(\beta) = (-1)^{m'+m+1} T_{\ell'\ell}^{m'm}(\beta), \tag{8}$$

$$R_{\ell'\ell}^{m',m}(\pi-\beta) = (-1)^{\ell'+\ell+m'+m} R_{\ell'\ell}^{m'm}(\beta), \quad H_{\ell'\ell}^{m',m}(\pi-\beta) = (-1)^{\ell'+\ell+m'+m} H_{\ell'\ell}^{m'm}(\beta),$$
$$T_{\ell'\ell}^{m',m}(\pi-\beta) = (-1)^{\ell'+\ell+m'+m+1} T_{\ell'\ell}^{m'm}(\beta), \tag{9}$$

Matrices R and H, whch specify instrumental response to poloidal vector fields, are real; matrix T is imaginary. Equation (9) shows that for poloidal fields (which describe undistorted eigenfunctions of solar oscillations) the amplitudes of the response coefficients of the instrument are identically zero when solar B-angle is zero and $\ell'+\ell+m'+m$ is odd; we refer to these leaks as "prohibited" leaks. For toroidal fields, situation is reverse: prohibited leaks are those with $\ell'+\ell+m'+m$ even. For prohibited leaks, the leak amplitude is an odd function of solar B-angle; for unprohibited leaks, it is even function of B. In power spectra, the magnitude of spatial leaks (absolute value of leak amplitude squared) is always an even function of solar B-angle, i.e. does not depend on its sign.

REFERENCES

Beck, J. G., & Schou, J., 2000, Solar Phys., 193, 333

Fleck, B., Couvidat, S., Straus, T., 2011, Solar Phys., 271, 27

12

Korzennik, S. G., 2005, ApJ, 626, 585

Korzennik, S. G., 2023, Frontiers in Astron. & Space Sci., 9, id.1031313

Larson, T. P., & Schou, J., 2015, Solar Phys., 290, 3221

Larson, T. P., & Schou, J., 2018, Solar Phys., 293, 29

Ritzwoller, M. H., & Lavely, E. M., 1991, ApJ, 369, 557

Schou, J., Christensen-Dalsgaard, J., Thompson, M. J., 1994, ApJ, 433, 389

Snodgrass, H. B., & Ulrich, R. K., 1990, ApJ, 351, 309

Vorontsov, S. V. 2007, MNRAS, 378, 1499

Vorontsov, S. V., & Jefferies, S. M., 2005, ApJ, 623, 1202

Vorontsov, S. V., & Jefferies, S. M., 2013, ApJ, 778, 75

Vorontsov, S. V., Christensen-Dalsgaard, J., Schou, J., Strakhov, V. N., Thompson, M. J., 2002, in: From Solar Min to Max: Half a Solar Cycle with SOHO, ed. A. Wilson, Proc. *SOHO* 11 Symposium (ESA SP-508; Noordwijk: ESA), 111